Acta Materialia 161 (2018) 352–359

Contents lists available at ScienceDirect

Acta Materialia

journal homepage: www.elsevier.com/locate/actamat

Full length article

Stable antiferroelectricity with incompletely reversible phase transition and low volume-strain contribution in $BaZrO_3$ and $CaZrO_3$ substituted $NaNbO_3$ ceramics

Ruzhong Zuo*, Jian Fu, He Qi

Institute of Electro Ceramics & Devices, School of Materials Science and Engineering, Hefei University of Technology, Hefei, 230009, PR China

ARTICLE INFO

Article history:
Received 7 July 2018
Received in revised form
21 September 2018
Accepted 24 September 2018
Available online 26 September 2018

Keywords:
Antiferroelectricity
$NaNbO_3$
Lead-free
Phase transition
Strains

ABSTRACT

In this work a reproducible double polarization versus electric field (P-E) hysteresis loop clearly reveals a room-temperature stable antiferroelectricity (AFE) in virgin $NaNbO_3$ (NN) samples doped with 6 mol% $BaZrO_3$ and 3 mol% $CaZrO_3$. Inconsistent but sprout-like strain versus field (S-E) curves without any negative strains between the first and non-first cycles yet display an incompletely reversible field induced AFE-ferroelectric (FE) phase transition. In/ex-situ synchrotron x-ray diffraction results suggest irrecoverable AFE states with orthorhombic and monoclinic structures before and after electric cycling, respectively, which generate an irreversible strain contribution including both irreversible volume (22%) and lattice (78%) strains. Frequency-dependent measurements of P/S-E curves demonstrate the rest of remanent strains from the time effect of back-switching from field induced FE to AFE equivalently existing in strain loops of any cycles at a fixed frequency. Compared with virgin samples, post-cycled samples exhibit a completely reversible monoclinic AFE-monoclinic FE phase transition but a relatively small poling strain. It is of particular note that the contribution of the volume strain to the poling strain is only 20% in AFE NN-based ceramics, in which a positive longitudinal strain and a negative transverse strain are concurrently observed, challenging a common knowledge that both strains in two directions should be positive for traditional Pb-based AFE ceramics. The experimental results provide new insights into the AFE phase stability of NN and an exciting possibility to take advantage of NN-based antiferroelectric ceramics for large-displacement actuators in future.

1. Introduction

Phase structure change in response to external electric fields has been observed in both antiferroelectric (AFE) and ferroelectric (FE) materials [1–5]. Particularly, AFE materials with antiparallel off-centering ionic displacements in neighboring unit cells are of particular interest because both a considerable expansion of the unit cell and a rapid increase in the polarization can be observed as an external electric field forces an AFE order to transform into a FE order [3–5]. Extensive researches have been so far reported on their potential applications in the field of large-displacement actuators and high power pulse capacitors [6–8]. Considering the environmental and health concerns from lead-based materials, lead-free FE or AFE alternatives have achieved extensive attention in the past decades [9–11].

Unfortunately, the selectable lead-free AFE material seems to be limited. Although $(Bi_{0.5}Na_{0.5})TiO_3$ (BNT)-based lead-free compositions were reported to exhibit giant strains and typical double-like P-E hysteresis loops [12,13], the relevant mechanism was not ascribed to the early-suggested field-induced AFE to FE phase transition [13] in the end, but to the field forced ergodic relaxor to long-range FE order later [14–16]. The property of high-temperature relaxor phases in BNT-based ceramics is still unclear. In addition, the rationality of the existence of AFE phase in BNT-based compositions was also challenged by their different strain behavior as compared with that of typical Pb-based AFE ceramics [14]. Among alkaline niobates, $NaNbO_3$ (NN) is a well-documented lead-free AFE material. Its room-temperature structure is commonly referred as the AFE P phase with an orthorhombic Pbma symmetry [10,17–19]. However, a polar orthorhombic phase ($P2_1ma$ symmetry of Q phase) was found to coexist with the AFE P phase owing to their comparable free energy [20–22], which tends

* Corresponding author.
E-mail address: piezolab@hfut.edu.cn (R. Zuo).

https://doi.org/10.1016/j.actamat.2018.09.056
1359-6454/

to make the pure NN ceramic exhibit FE-like square P-E loops as a result of an irreversible field-induced AFE to FE phase transition. A lot of attempts have been focused on increasing the stabilization of the AFE phase over the FE phase in NN-based ceramics through suitable composition modification. A typical double P-E loop can be observed in these modified NN-based AFE ceramics [23–27]. It is thus reasonable to expect highly reversible strain values in these materials. Unfortunately, the strain characteristic of these compositions in response to the stimuli of external electric fields has been rarely investigated till now. It would be of much interest to make clear how the field induced strain behaviors and what the relation between the strain feature and the phase structure variation is.

In the present study, the antiferroelectricity of NN ceramics was stabilized by co-doping 6 mol% $BaZrO_3$ (BZ) and 3 mol% $CaZrO_3$ (CZ). The ceramic sample exhibits a particular AFE-FE phase transition behavior as characterized by reversible P-E hysteresis loops, but incompletely reproducible bipolar S-E curves during electric field loading. The underlying strain mechanism was explored by combining in/ex-situ synchrotron x-ray diffraction (XRD) with the corresponding dielectric, ferroelectric and strain measurements.

2. Experimental

The 0.91NN-0.06BZ-0.03CZ ceramic was fabricated using a conventional solid-state reaction method. Raw powders of high-purity Na_2CO_3 (>99%), Nb_2O_5 (>99%), $BaCO_3$ (>99%), $CaCO_3$ (>99%) and ZrO_2 (>99%) were weighed according to the chemical formula, and ball-milled for 8 h in ethanol with zirconia balls. The dried powders were calcined at 850 °C for 3 h and then ball milled again for 10 h. The powder was pressed into pellets with 10 mm in diameter and then sintered in sealed crucibles at 1350–1375 °C for 2 h. The sample density was measured by the Archimedes method. The major surfaces of the sintered pellets were well polished, then coated with silver paste and finally fired at 550 °C for 30 min. The ceramic samples were ground and polished, and then annealed at 500 °C for 4 h to remove mechanical stress. Conductive adhesives (or silver paste) were screened on two major polished surfaces.

The crystal structure of the as-sintered (virgin) and poled (i.e., after electric cycling at 20 kV/mm) ceramic powders was examined by means of synchrotron XRD at beam line TPS-09A of National Synchrotron Radiation Research Center (NSRRC, Hsinchu, Taiwan). Beam energy of 20 keV ($\lambda = 0.619926$ Å) was selected and the data were recorded by position-sensitive detector MYTHEN 24 K for the Rietveld refinement. The ceramic powder was loaded into a 0.2–0.5 mm capillary for uniform absorption and faster rotation during data collection. Dielectric properties for both poled and unpoled samples were measured as a function of temperature and frequency by an LCR meter (Agilent E4980A, Santa Clara, CA). The polarization versus electric field (P-E) and strain versus electric field (S-E) curves were measured by using a ferroelectric measuring system (Precision multiferroelectric, Radiant Technologies Inc., Albuquerque, NM) with an accessory laser interferometer vibrometer (AE SP-S 120E, SIOS Mebtechnik, GmbH, Ilmenau, Germany). For in-situ synchrotron XRD measurement, thin gold electrodes were sputtered onto two well-polished sides of the ceramic disk. The measurements were carried out at Shanghai Synchrotron Radiation Facility (SSRF) using beam line 14B1 with a beam energy of 10 keV ($\lambda = 1.2398$ Å). For comparison, the (200) pseudo-cubic reflection line of the crushed sample after poling was also recorded at SSRF. The domain morphology observation and selected area electron diffraction (SAED) were performed on a transmission electron microscope (TEM) (JEM-ARM200F, JEOL, Japan) operated at 200 kV. For TEM examination, samples were first mechanically polished to a thickness of ~20 μm and then ion-milled on a Precision Ion Polishing System (PIPS, Model 691, Gatan Inc., Pleasanton, CA) at 5 kV. All specimens were annealed at 80 °C for at least one day to release the mechanical stress before the observation.

3. Results and discussion

Fig. 1(a and b) shows the grain and domain morphology of the 0.91NN-0.06BZ-0.03CZ ceramic sintered at its optimal temperature, respectively. The sample exhibits a dense and uniform microstructure with an average grain size of ~4.8 μm and a high relative density of more than 96%.

At ambient conditions, NN is commonly recognized as an AFE P phase, but the metastable FE Q phase may coexist with P phase in a variety of ways because of a comparable free energy profile between them. In the present study, a typical AFE domain morphology can be observed. This can be confirmed by the occurrence of the 1/4 type superstructure shown in the inset of Fig. 1(b), which is caused by the quadrupled unit cell of P phase along the [0l0] direction as a result of the pairs of alternating layers with $a^-b^+a^-$ and $a^-b^-a^-$ oxygen octahedral tilting [17]. The result indicates that that AFE phase has been effectively stabilized by co-doping BZ and CZ.

The stabilized antiferroelectricity in the 0.91NN-0.06BZ-0.03CZ sample can be also demonstrated by looking at its dielectric and ferroelectric behavior, as shown in Fig. 1(c and d). Only a dielectric anomaly around 200 °C denoting the phase transition between the AFE P phase and the paraelectric cubic phase can be observed for both virgin and poled samples. Both of them look almost the same, apart from a bit smaller dielectric maximum for the poled sample, indicating that the electric field induced AFE to FE phase transition is reversible basically but incompletely, as shown in Fig. 1(c). In the case of irreversible AFE-FE phase transition [19], a significant increase of dielectric maximum can be clearly observed in NN-based ceramics after poling. Moreover, the dielectric maximum of the virgin sample in this study was found to be even smaller than that of typical NN-based ferroelectrics and even pure NN ceramics [19], possibly due to the vanishing of the FE Q phase in the 0.91NN-0.06BZ-0.03CZ sample. Fig. 1(d) compares bipolar P-E loops of the first and second cycles and the corresponding polarization current density (J) as a function of electric field. The well-reproducible double P-E hysteresis loops with high saturate polarization and four current density peaks (P_1, P_2, P_1' and P_2') can be observed in both first and second cycles. These results indicate that a FE order can be established under a high external electric field. However, the field-induced FE order is metastable, and cannot be maintained after removal of electric field. Because of this, the electric field induced AFE to FE phase transition also proves to be reversible to some extent in BZ and CZ doped NN ceramics.

Fig. 2(a and b) shows the first and second-cycle bipolar S-E curves at 10 Hz of the 0.91NN-0.06BZ-0.03CZ sample, respectively, which can provide the electric field induced longitudinal strain (S_L), transverse strain (S_T), and the resulting volume strain (S_V) in the corresponding cycle. It is found that in the first cycle, the electric field induced S_{L1} is very large with a value of as high as ~0.45%. However, such a high strain value cannot be sustained and only a relatively low S_{L2} value of ~0.327% in the second cycle can be observed. Similarly, both the absolute values of S_T and S_V show a decrease of different degrees in the second cycle. In addition, it is worthy of note that the sample exhibits asymmetric S-E curves with a large strain gap on the left side of S-E curves in the first cycle. The different thing is that a typical butterfly-like S-E curve can be observed after poling in the case of NN-based AFE ceramics with an irreversible phase transition [19]. By comparison, only sprout-like S-E curves with no detectable negative strains can be observed in Fig. 2(b). Interestingly, the value of strain gap (S_{g2}) in the second

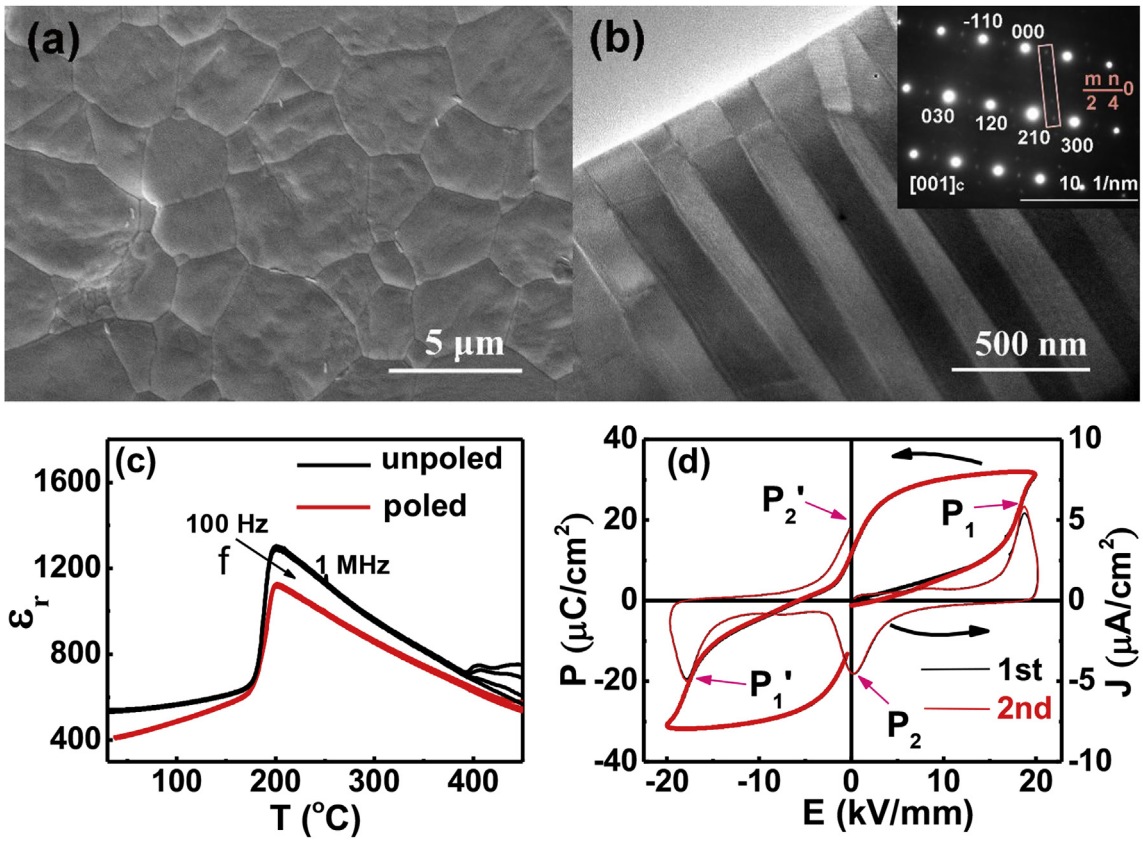

Fig. 1. The grain (a) and domain (b) morphology of the 0.91NN-0.06BZ-0.03CZ ceramic sample, (c) the dielectric permittivity as a function of temperature and frequency for both unpoled and poled samples, and (d) bipolar P-E loops and corresponding J-E curves as a function of the applied electric field at 10 Hz during the first and second cycles. The inset in (b) shows the corresponding SAED pattern.

electric field cycle is much less than the value (S_{g1}) in the first cycle, and the difference between S_{g1} and S_{g2} (S_{g1}-S_{g2}) is just equal to the difference between S_{L1} and S_{L2} (S_{L1}-S_{L2}), as shown in Fig. 2(c), meaning that the same strain magnitude as S_{g2} can be involved in the S_{g1} value. In addition, the S_{g2} can be repeated in each electric cycle after poling, as shown in Fig. 3. As a result, it is clear that the strain gap S_{g1} on the left side of the first-cycle loop should be composed of two independent parts. The one is related to the field induced irreversible change between the initial and poled AFE states (S_{L1}-S_{L2}, or S_{g1}-S_{g2}). The other part (S_{g2}) probably results from the time hysteresis effect of the back switching from field induced FE phase to the AFE phase, instead of the texturing effect of poled AFE phases [28]. This is also responsible for the observed remanent polarization (P_r) in Fig. 1(d). This judgement can be supported by frequency-dependent strain and polarization measurements, in which both the strain gap S_{g2} (or remanent strain S_{r2}) and the P_r value gradually disappear with decreasing the measuring frequency (see Fig. 4). The textured AFE states might produce an irreversible strain but should not generate a P_r value. If one carefully looks at Fig. 1(d), P_r is not zero but completely repeatable ($\Delta P_r = 0$) during different electric cycles including the first cycle, further indicating that field induced AFE-FE phase transition is reversible only in the sense of the polarization. By comparison, the remanent strain (S_r) is not zero but totally different ($\Delta S_r \neq 0$) between the first cycle and non-first cycles. As a result, a small repeatable S_r during the second cycle and even after the second cycle should be also attributed to the time hysteresis effect of FE back to AFE phases. An irreversible change existing during the first cycle results in a big S_r as observed in Fig. 2(a), but does not contribute to the P_r value.

On the other hand, it can be seen from Fig. 2(a and b) that the S_T value in the 0.91NN-0.06BZ-0.03CZ AFE ceramic is negative in both the first and second cycles, which is different from typical lead-based AFE ceramics with reversible AFE-FE phase transition [29,30]. It is a common phenomenon in lead-based AFEs that the lattice parameter c_T in the AFE tetragonal phase is smaller than the a_R value in the field induced rhombohedral FE phase. In the meantime, the c axis of domains in AFE phase is preferentially oriented perpendicular to the electric field direction after the electric field loading [5,31]. Both of them tend to cause the observed expansion along the transverse direction. However, this kind of relationship usually observed in lead-based AFE compositions seems to not exist in the lead-free AFE 0.91NN-0.06BZ-0.03CZ sample possibly because of different phase structures and different electric-field induced phase transition behavior.

Fig. 5(a and b) depicts the observed, calculated, and difference profiles of as-sintered and poled 0.91NN-0.06BZ-0.03CZ ceramic powders by means of the Rietveld refinement of the synchrotron XRD data using the GSAS software. It can be seen that the overall fit between the observed and calculated profiles for virgin ceramic powders is very good based on an orthorhombic Pbma symmetry. However, this mode cannot be suitable for the poled ceramic powder. Other possible structural models such as orthorhombic Pmnm and $P222_1$, and monoclinic $P2_1$ have been also tried in current work. However, the poor fit suggests that the former two orthorhombic symmetries are still not suitable for describing the structure of the poled ceramic powder. By comparison, the XRD pattern of the poled powder can be well fitted by using the $P2_1$ symmetry. Table 1 gives a set of refinement structural parameters including lattice parameters and unit cell volume, and reliability

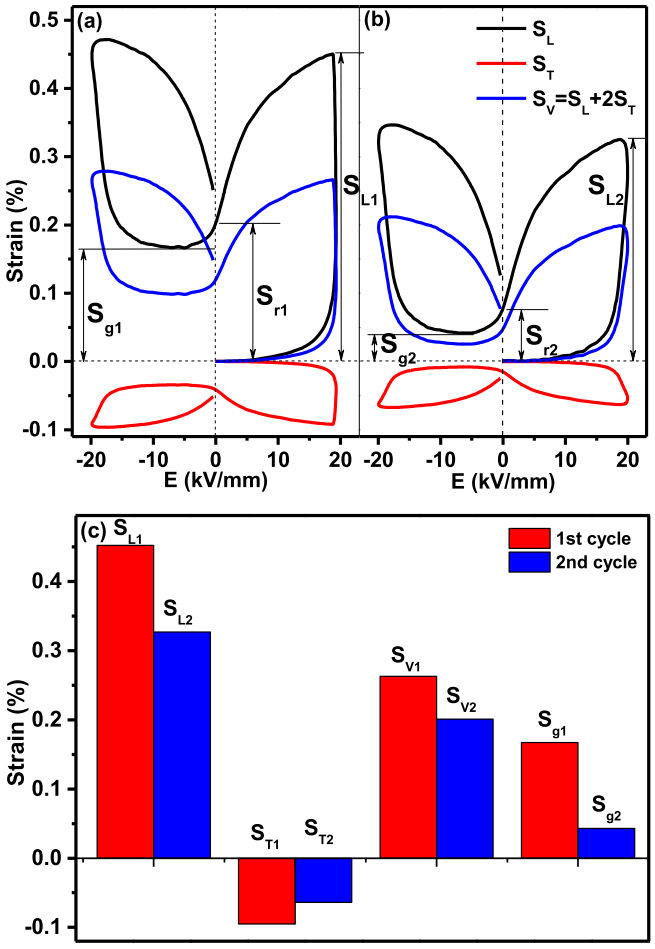

Fig. 2. The longitudinal strain S_L, transverse strain S_T and the corresponding volume strain S_V during the (a) first and (b) second cycles at 10 Hz for the 0.91NN-0.06BZ-0.03CZ ceramic, and (c) the comparison of various strains between the first and second cycles (the numbers 1 and 2 refer to the first and second cycles, respectively).

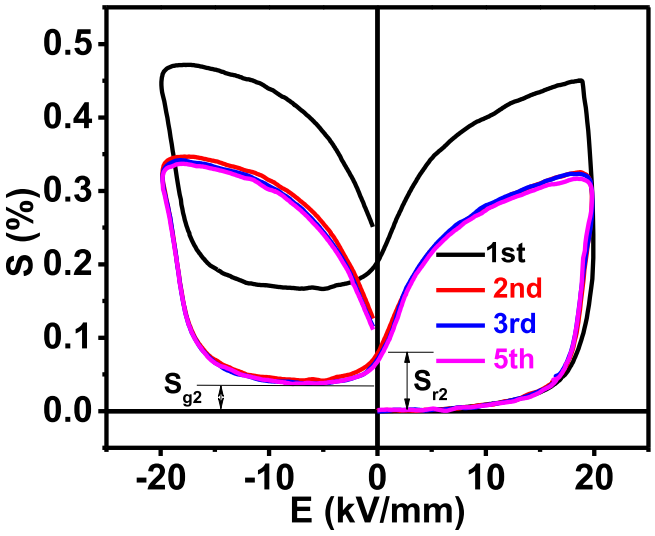

Fig. 3. Bipolar S-E curves of the 0.91NN-0.06BZ-0.03CZ ceramic sample measured at different electric cycles at 10 Hz.

factors of R_{wp}, R_p, and χ^2, in which R_{wp} is the reliability factor of weighted patterns, R_p is the reliability factor of patterns and χ^2 is

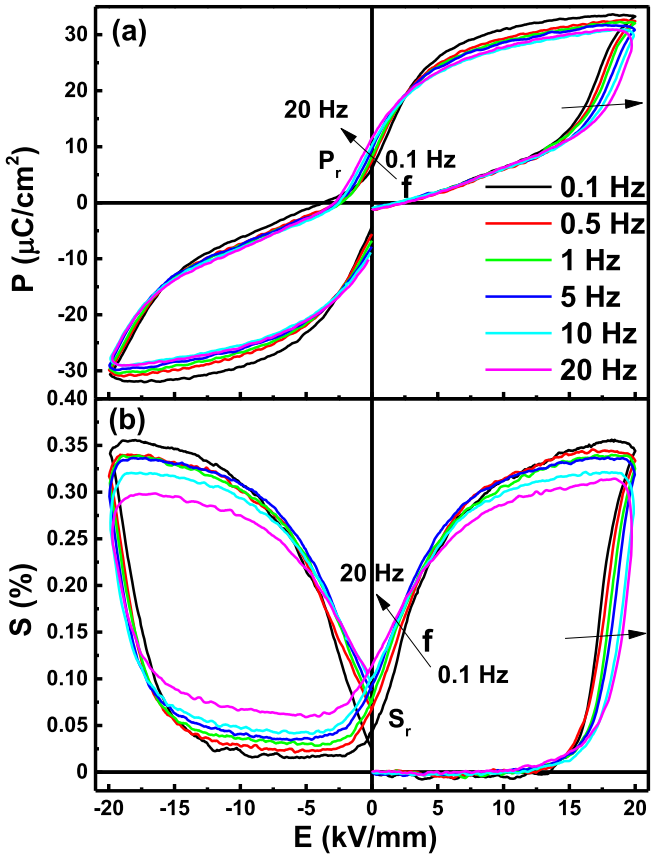

Fig. 4. Bipolar P-E and S-E curves measured at different frequencies after the first electric cycle for the 0.91NN-0.06BZ-0.03CZ ceramic sample.

the goodness-of-fit indicator. Fig. 6 depicts the schematic crystallographic structures of Pbma and $P2_1$ symmetries, In the $P2_1$ symmetry, the Nb cation displacements are antiparallel to the direction perpendicular to the pseudo-cubic b axis [32]. However, compared with the orthorhombic Pbma symmetry, $P2_1$ symmetry belongs to a typical monoclinic structure, in which pairs of alternating layers with two kinds of octahedral tilts labeled as $a^-b^+c^-$ and $a^-b^-c^-$ exist, instead of the $a^-b^+a^-$ and $a^-b^-a^-$ octahedral tilts in Pbma symmetry [33]. As a result, the antiparallel cation displacement in $P2_1$ symmetry is along the [u0w] ($u \neq w$) direction in the (010) plane, which can be considered as a slight deviation from the [101] polarization vectors in Pbma symmetry. The Rietveld refinement results in Table 1 indicate that the unit cell volume of the AFE orthorhombic phase is slightly smaller than that of the AFE monoclinic phase. The volume strain (~0.079%) calculated from their subcells difference between the initial and poled AFE states (primitive pseudo-cubic cell = V/8) in Table 1 was found to approximate to the difference between S_{V1} and S_{V2} in Fig. 2(c), which contributes to an irreversible linear strain of ~0.025% ($\frac{1}{3}(S_{V1}-S_{V2})$) in a total value of ~0.125% ($S_{L1}-S_{L2}$), indicating that there must be other irreversible strain contributions.

For better understanding the structural origin of irreversible strains during the field-induced phase transition, in/ex-situ high-resolution synchrotron XRD measurement was carried out under different external field loading conditions. Fig. 7 (a, b) shows the evolution of (200) and (220) pseudo-cubic reflections under different electric field conditions from a virgin state. To simplify the data analysis, both AFE orthorhombic and monoclinic phases were described as a pseudo-cubic primitive unit cell with $a \approx \sqrt{2}a_{pc}$, $c \approx \sqrt{2}c_{pc}$, and $b \approx 4b_{pc}$. It can be seen from Fig. 7(a) that a typical

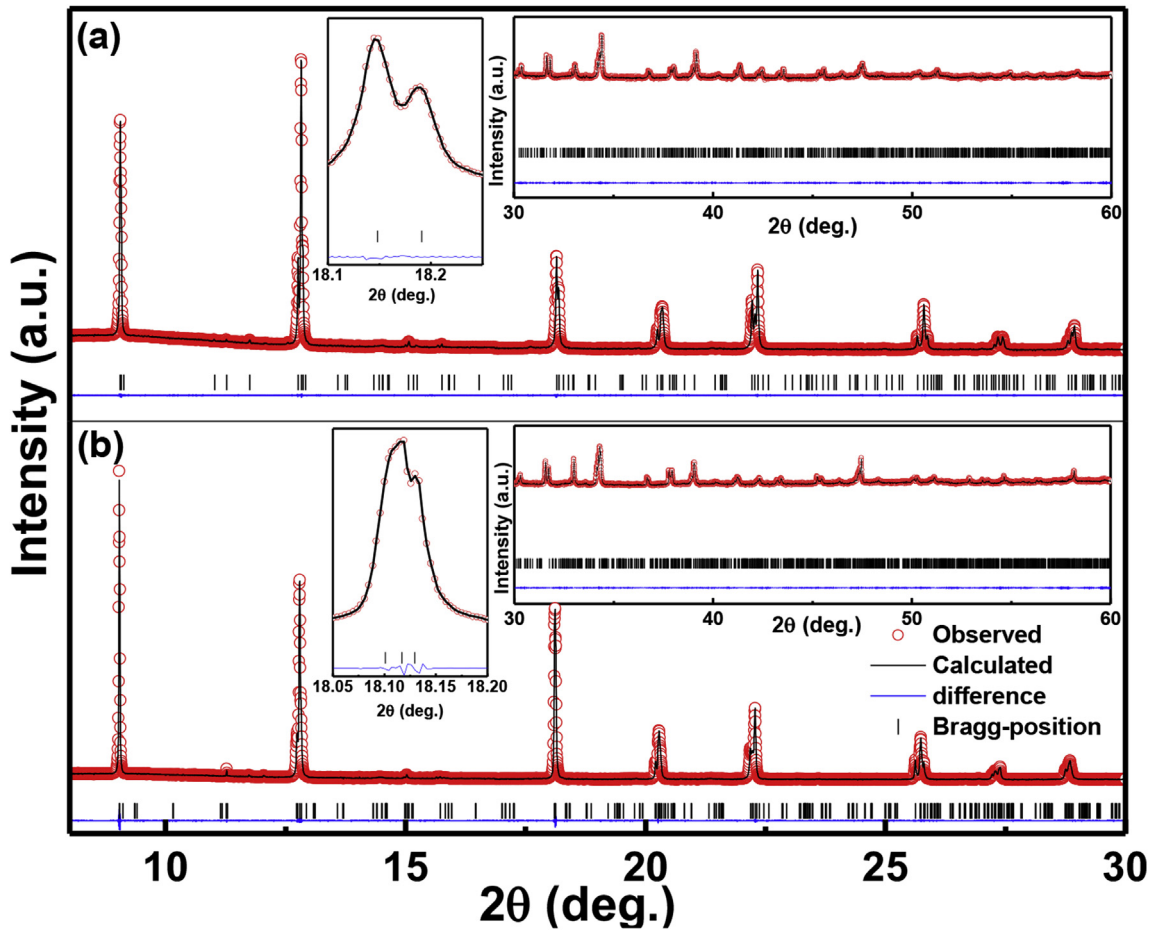

Fig. 5. Rietveld structural refinement patterns of (a) unpoled (as-sintered) and (b) poled 0.91NN-0.06BZ-0.03CZ ceramic powders. The inset shows the fitting results of the (200) pseudo-cubic reflection lines and the view of Rietveld fits at the high Bragg-angle range.

Table 1
Refined structural parameters of the as-sintered (unpoled) and poled 0.91NN-0.06BZ-0.03CZ ceramic powders.

samples	Space group	Lattice parameters	V (Å^3)	R_{wp} (%)	R_p (%)	χ^2
Unpoled	Pbma	a = 5.5578(3) Å, b = 15.6279(6) (Å), c = 5.5071(4) (Å), α = 90°, β = 90°, γ = 90°	478.33	9.28	6.73	3.25
Poled	$P2_1$	a = 5.5601(6) Å, b = 15.6265(2) (Å), c = 5.5098(4) (Å), α = 90°, β = 90.31°, γ = 90°	478.71	10.28	7.72	3.47

AFE orthorhombic phase was identified in the virgin sample, as characterized by the $(002)_o(200)_o/(020)_o$ doublet and $(20\ -2)_o/(202)_o/(220)_o$ triplet. With increasing the electric field amplitude, the AFE orthorhombic domain orientation occurs until E = 10 kV/mm, beyond which the $(002)_o/(200)_o$ peak shows an obvious splitting, accompanied by the $(202)_o$ peak splitting. The observed peak splitting should be attributed to the transition of the cation displacement from antiparallel to parallel modes and the transition of the polar axis from [101] direction to [u0w] direction. As a result, the AFE orthorhombic phase tends to transform into the FE order with a monoclinic phase at 20 kV/mm starting from 10 kV/mm. After removal of electric field, it can be found that both c and a axis show an obvious shrinkage due to the shift of $(002)_m$ and $(200)_m$ peaks to higher-angle side, as shown in Fig. 7(c). At the same time, an obvious splitting of $(002)_m$ and $(200)_m$ peaks can be always observed. This indicates that the field-induced metastable FE monoclinic phase transforms into an AFE monoclinic phase (poled-1) instead of switching back to its initial AFE orthorhombic phase as external fields are totally released. Simultaneously, both a and c axes exhibit a gradual shrinkage as a result of the constriction effect of the unit cell in the ac plane. For the second cycle shown in Fig. 7(b), an obvious AFE monoclinic to FE monoclinic phase transition occurs as E > 10 kV/mm, below which only the domain orientation of the AFE monoclinic phase can be observed. During the phase transition, both $(002)_m$ and $(200)_m$ peaks shift to the lower-angle side and accompany an abrupt change of $(002)_m$ and $(200)_m$ peak intensities. After the applied field is removed, an AFE monoclinic phase can be totally recovered if one compares the XRD data for poled-1 and poled-2 states in Fig. 7(d), indicating that the field induced AFE monoclinic-FE monoclinic phase transition is completely reversible after the first cycle. Compared with the freely-oriented powder sample (the crushed sample after poling), no any obvious domain preferential orientation along the field direction can be observed in the AFE monoclinic phase of the ceramic disk after the first or second electric cycle, as shown in Fig. 8. This further supports the above interpretation concerning the origin of S_{g2} observed in Figs. 2 and 3.

The profiles of the (200) pseudo-cubic reflection under different electric field conditions were fitted by means of the pseudo-Voigt function (see Fig. 7(c and d)), from which the lattice strain (S_{latt})

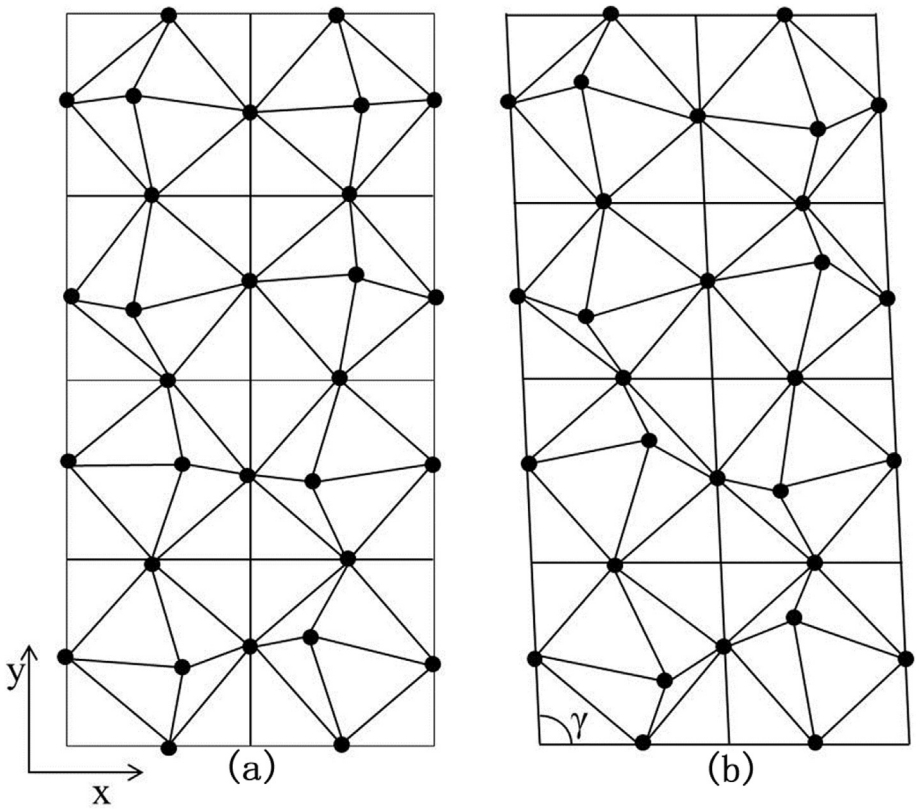

Fig. 6. Schematic crystal structures for (a) AFE orthorhombic Pbma and (b) AFE monoclinic $P2_1$ phases (Only oxygen atoms are denoted by black solid dots).

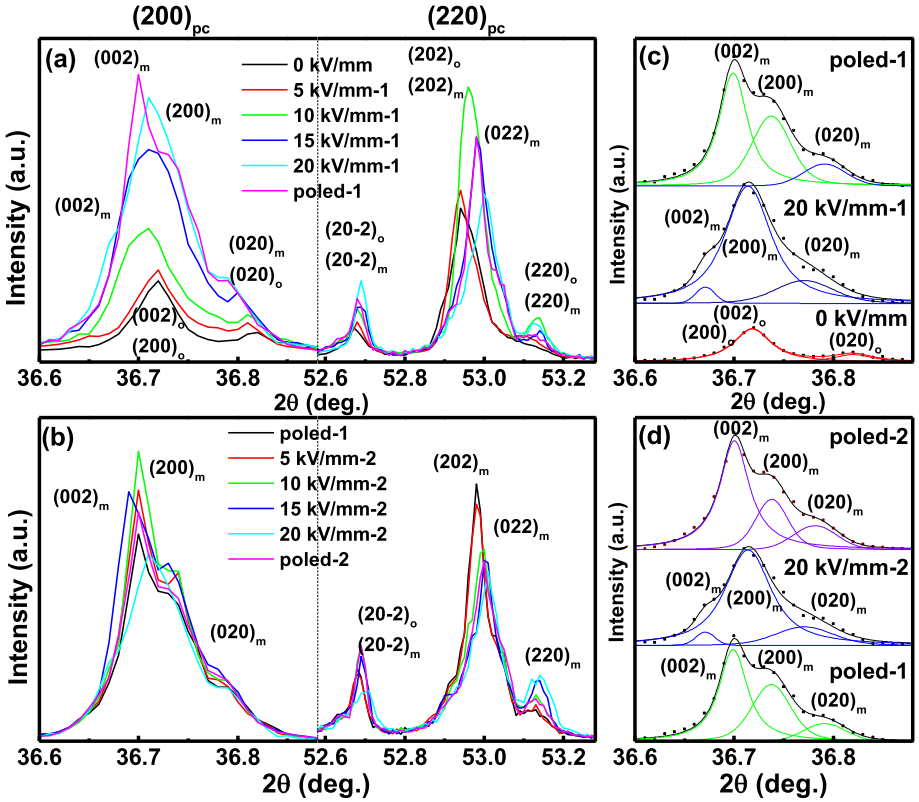

Fig. 7. Evolution of $(200)_{pc}$ and $(220)_{pc}$ reflections under various electric fields for the 0.91NN-0.06BZ-0.03CZ sample during the (a) first and (b) second electric cycles, and the fitting results of the $(200)_{pc}$ reflections under different electric field conditions during or after the (c) first and (d) second electric cycles, respectively. The poled-1 and poled-2 stand for the states as the applied electric field is totally released after the first and second cycles, respectively.

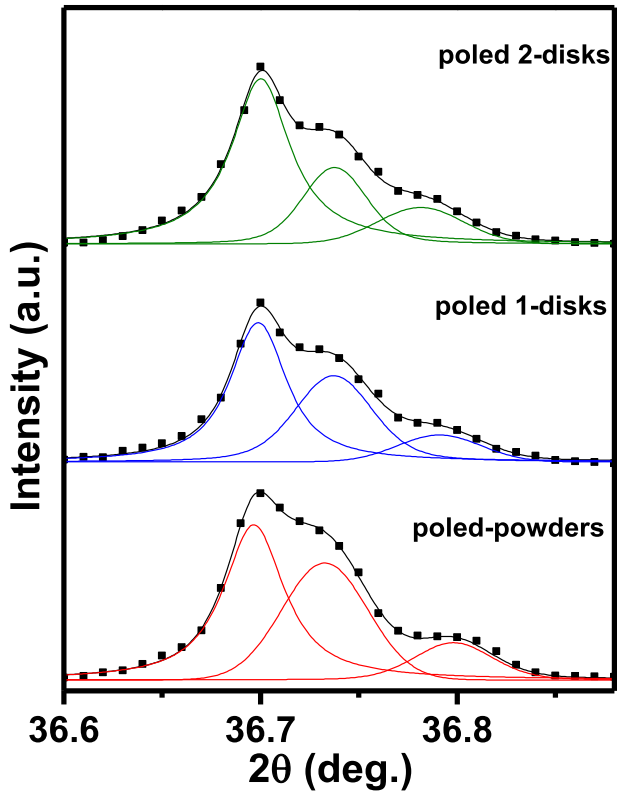

Fig. 8. The comparison of the (200) pseudo-cubic reflections for the 0.91NN-0.06BZ-0.03CZ sample under different conditions as indicated. The poled-1 and poled-2 stand for the states as the applied electric field is totally released after the first and second cycles, respectively. The poled powder is from the crushed disk after poling.

can be semiquantitatively estimated, as shown in Fig. 9. The lattice strains during the first cycle ($S_{latt\text{-}1}$) and the second cycle ($S_{latt\text{-}2}$) are found to be as high as ~0.166% and ~0.077%, respectively, which contribute to an irreversible lattice strain ($S_{latt\text{-}ir} = S_{latt\text{-}1}\text{-}S_{latt\text{-}2}$) of ~0.089% between the first and second cycle, according to the equation $S_{latt-1} = \frac{d_{(002)m|20kV/mm} - d_{(002)o|virgin}}{d_{(002)o|virgin}} \times 100\%$ (first cycle) and $S_{latt-2} = \frac{d_{(002)m|20kV/mm} - d_{(002)m|poled}}{d_{(002)m|poled}} \times 100\%$ (second cycle). This part of irreversible strains ($(S_{latt\text{-}1}\text{-}S_{latt\text{-}2})$) plus irreversible volume strain

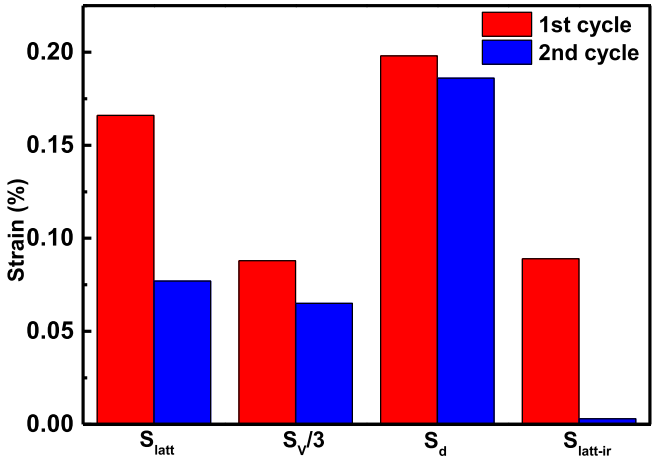

Fig. 9. The variation of S_{latt}, $S_v/3$, S_d and $S_{latt\text{-}ir}$ between the first and second cycles obtained from the corresponding XRD data in Fig. 7 and bipolar S-E curves in Fig. 2.

contribution ($(S_{V1}\text{-}S_{V2})/3 = 0.025\%$) just approximates to the observed strain difference ($S_{L1}\text{-}S_{L2}$) in Fig. 2. In other words, the strain gap difference between first and second cycles ($S_{g1}\text{-}S_{g2}$) should be mainly attributed to irreversible lattice strains and volume strains during the field induced AFE-FE phase transition. Compared with the volume strain, the irreversible lattice strain (~78%) during the phase transition is dominant. In addition to the lattice strain and volume strain, the rest of contributions to the poling strain during the first cycle or the second cycle should be from the domain switching (S_d) as characterized by the variation of diffraction peak intensities in Fig. 7. According to the calculated lattice strains and measured volume strains, we can roughly estimate S_d values during the first and second cycle, respectively, as shown in Fig. 9. It can be found that the ceramic exhibits high S_d values in both first (~0.198%) and second (~0.186%) cycles. It seems that S_d shows little dependence on electric field cycling and thus the strain contribution of domain switching should be reversible, although the initial phase structure shows an irreversible change after poling. By comparison, both lattice and volume strains show an obvious decrease after the first cycle. In addition, the contribution of the volume strain to the poling strain either during the first cycle or during the second cycle is small (~20%). This phenomenon is much different from that observed in typical lead-based perovskite AFE ceramics, in which the volume strain contribution can reach up to ~80%. Therefore, further modification of the NN-based antiferroelectric ceramic would be definitely necessary in order to fully utilize application potentials although its antiferroelectricity has been generally stabilized.

4. Conclusions

A stabilized antiferroelectricity was found out in the lead-free 0.91NN-0.06BZ-0.03CZ ceramic, which exhibits a particular field-induced AFE-FE phase transition as characterized by a reversible P-E loop but an irreproducible bipolar S-E curve. In/ex-situ synchrotron XRD results indicate that the studied composition owns an AFE orthorhombic phase structure at its virgin state, and can transform into a metastable FE order with a monoclinic symmetry under a strong external electric field. After removal of the electric field, an AFE order with a monoclinic symmetry rather than the initial AFE orthorhombic phase can be observed. A reversible AFE monoclinic to FE monoclinic phase transition occurs repeatedly only after the first electric cycle. Incomplete reversibility of the initial AFE orthorhombic to AFE monoclinic phase transition makes the S-E curve of the first cycle severely asymmetric with a large strain gap because of an irreversible process between the initial and poled AFE states. Frequency-dependent P/S-E curves strongly support the fact that a little P_r and a small S_r (or the strain gap on the left) from non-first cycles should be due to the time effect of back-switching from the field induced FE monoclinic to the AFE monoclinic phase, instead of the texturing effect of poled AFE states, in combination with the XRD result of samples with different states. Irreversible changes between the first and second cycles, which are responsible for the decrease of poling strain after the first cycle, are dominated by both an irreversible lattice strain (78%) and an irreversible volume strain (22%). Compared with traditional Pb-based AFE materials, a relatively small volume strain contribution of only 20% in NN-based AFE ceramics deserves a particular note, in which a positive longitudinal strain and a negative transverse strain are unexpectedly observed, challenging a common knowledge in traditional Pb-based AFE materials. The experimental results demonstrate an exciting possibility to utilize NN-based antiferroelectric ceramics for large-displacement actuators in future by further modifying the AFE phase structure.

Acknowledgements

This work was supported by the National Natural Science Foundation of China (Grants No. 51472069). In addition, we acknowledge the support from Dr. H. S. Sheu, Dr. Y. C. Chuang, Dr. Y. C. Lai and Mr. C. K. Chang for the experiment assistance at TPS 09A.

References

[1] H. Liu, J. Chen, L.L. Fan, Y. Ren, Z. Pan, K.V. Lalitha, J. Rodel, X.R. Xing, Critical role of monoclinic polarization rotation in high-performance perovskite piezoelectric materials, Phys. Rev. Lett. 119 (2017), 017601.
[2] H. Liu, J. Chen, H.B. Huang, L.L. Fan, Y. Ren, Z. Pan, J.X. Deng, L.Q. Chen, X.R. Xing, Role of reversible phase transformation for strong piezoelectric performance at the morhpotropic phase boundary, Phys. Rev. Lett. 120 (2018), 055501.
[3] C. Kittel, Theory of antiferroelectric crystals, Phys. Rev. 82 (1951) 729–732.
[4] L.E. Cross, Antiferroelectric-ferroelectric switching in a simple 'Kittel' antiferroelectric, J. Phys. Soc. Jpn. 23 (1967) 77–82.
[5] S.E. Park, M.J. Pan, K. Markowski, S. Yoshikaw, L.E. Cross, Electric field induced phase transition of antiferroelectric lead lanthanum zirconate titanate stannate ceramics, J. Appl. Phys. 82 (1997) 1798–1803.
[6] W.Y. Pan, C.Q. Dam, Q.M. Zhang, L.E. Cross, Large displacement transducers based on electric field forced phase transitions in the tetragonal $(Pb_{0.97}La_{0.02})(Ti,Zr,Sn)O_3$ family of ceramics, J. Appl. Phys. 66 (1989) 6014–6023.
[7] R. Xu, B.R. Li, J.J. Tian, Z. Xu, Y.J. Feng, X.Y. Wei, D. Huang, L.J. Yang, $Pb_{0.94}La_{0.04}[(Zr_{0.70}Sn_{0.30})_{0.90}Ti_{0.10}]O_3$ antiferroelectric bulk ceramics for pulsed capacitors with high energy and power density, Appl. Phys. Lett. 110 (2017) 142904.
[8] L. Zhao, Q. Liu, J. Gao, S.J. Zhang, J.F. Li, Lead-free antiferroelectric silver niobate tantalite with high energy storage performance, Adv. Mater. 18 (2017) 1701824.
[9] Y. Saito, H. Takao, T. Tani, T. Nonoyama, K. Takatori, T. Homma, T. Nagaya, M. Nakamura, Lead-free piezoceramics, Nature 432 (2004) 84–87.
[10] X.L. Tan, C. Ma, J. Frederick, S. Beckman, K.G. Webber, The antiferroelectric-ferroelectric phase transition in lead-containing and lead-free perovskite ceramics, J. Am. Ceram. Soc. 94 (2011) 4091–4107.
[11] J. Rodel, W. Jo, K.T.P. Seifert, E.M. Anton, T. Granzow, D. Damjanovic, Perspective on the development of lead-free piezoceramics, J. Am. Ceram. Soc. 92 (2009) 1153–1177.
[12] R.Z. Zuo, C. Ye, X.S. Fang, J.W. Li, Tantalum doped $0.94Bi_{0.5}Na_{0.5}TiO_3$-$0.06BaTiO_3$ piezoelectric ceramics, J. Eur. Ceram. Soc. 28 (2008) 871–877.
[13] S.T. Zhang, A.B. Kounga, W. Jo, C. Jamin, K. Seifert, T. Granzow, J. Rodel, D. Damjanovic, High-strain lead-free antiferroelectric electrostrictors, Adv. Mater. 21 (2009) 4716–4720.
[14] W. Jo, R. Dittmer, M. Acosta, J.D. Zang, C. Groh, E. Sapper, K. Wang, J. Rodel, Giant electric-field-induced strains in lead-free ceramics for actuator applications-status and perspective, J. Electroceram. 29 (2012) 71–93.
[15] H. Simons, J.E. Daniels, J. Glaum, A.J. Studer, J.L. Jones, M. Hoffman, Origin of large recoverable strain in $0.94(Bi_{0.5}Na_{0.5})TiO_3$-$0.06BaTiO_3$ near the ferroelectric-relaxor transition, Appl. Phys. Lett. 102 (2013), 062902.
[16] T.Y. Li, X.J. Lou, X.Q. Ke, S.D. Cheng, S.B. Mi, X.J. Wang, J. Shi, X. Liu, G.Z. Dong, H.Q. Fan, Y.Z. Wang, X.L. Tan, Giant strain with low hysteresis in A-site-deficient $(Bi_{0.5}Na_{0.5})TiO_3$-based lead-free piezoceramics, Acta Mater. 128 (2017) 337–344.
[17] A.C. Sakowski-Cowley, K. Lukaszewicz, H.D. Megaw, The structure of sodium niobate at room temperature, and the problem of reliability in pseudosymmetric structures, Acta Crystallogr. 25 (1969) 851–865.
[18] L.S. Gao, H.Z. Guo, S.J. Zhang, C.A. Randall, A perovskite lead-free antiferroelectric $xCaHfO_3$-$(1-x)NaNbO_3$ with induced double hysteresis loops at room temperature, J. Appl. Phys. 120 (2016) 204102.
[19] M.X. Dou, J. Fu, R.Z. Zuo, Electric field induced phase transition and accompanying giant poling strain in lead-free $NaNbO_3$-$BaZrO_3$ ceramics, J. Eur. Ceram. Soc. 38 (2018) 3104–3110.
[20] S.K. Mishra, N. Choudhury, S.L. Chaplot, P.S.R. Krishna, R. Mittal, Competing antiferroelectric and ferroelectric interactions in $NaNbO_3$: neutron diffraction and theoretical studies, Phys. Rev. B 76 (2007), 024110.
[21] K.E. Johnston, C.C. Tang, J.E. Parker, K.S. Knight, P. Lightfoot, S.E. Ashbrook, The polar phase of $NaNbO_3$: a combined study by powder diffraction, solid-state NMR, and first-principles calculations, J. Am. Chem. Soc. 132 (2010) 8732–8746.
[22] J. Koruza, P. Groszewicz, H. Breitzke, G. Buntkowsky, T. Rojac, B. Malic, Grain-size-induced ferroelectricity in $NaNbO_3$, Acta Mater. 126 (2017) 77–85.
[23] Y.H. Xu, W. Hong, Y.J. Feng, X.L. Tan, Antiferroelectricity induced by electric field in $NaNbO_3$-based lead-free ceramics, Appl. Phys. Lett. 104 (2014), 052903.
[24] H.Z. Guo, H. Shimizu, Y. Mizuno, C.A. Randall, Strategy for stabilization of the antiferroelectric phase (Pbma) over the metastable ferroelectric phase ($P2_1ma$) to establish double loop hysteresis in lead-free $(1-x)NaNbO_3$-$xSrZrO_3$ solid solution, J. Appl. Phys. 117 (2015) 214103.
[25] H. Shimizu, H.Z. Guo, S.E. Reyes-Lillo, Y. Mizuno, K.M. Rabe, C.A. Randall, Lead-free antiferroelectric: $xCaZrO_3$-$(1-x)NaNbO_3$ system ($0 \leq x \leq 0.10$), Dalton Trans. 44 (2015) 10763–10772.
[26] L.M. Chao, Y.D. Hou, M.P. Zheng, M.K. Zhu, High dense structure boosts stability of antiferroelectric phase of $NaNbO_3$ polycrystalline ceramics, Appl. Phys. Lett. 108 (2016) 212902.
[27] L.S. Gao, H.Z. Guo, S.J. Zhang, C.A. Randall, Stabilized antiferroelectricity in $xBiScO_3$-$(1-x)NaNbO_3$ lead-free ceramics with established double hysteresis loops, Appl. Phys. Lett. 112 (2018), 092905.
[28] T. Lu, A.J. Studer, L. Noren, W. Hu, D. Yu, B. McBride, Y. Feng, R.L. Withers, H. Chen, Z. Xu, Y. Liu, Electric-field-induced AFE-FE transitions and associated strain/preferred orientation in antiferroelectric PLZST, Sci. Rep. 6 (2015) 23659.
[29] W. Pan, Q.M. Zhang, A. Bhalla, L.E. Cross, Field-forced antiferroelectric-to-ferroelectric switching in modified lead zirconate titanate stannate ceramics, J. Am. Ceram. Soc. 72 (1989) 571–578.
[30] J. Frederick, X.L. Tan, W. Jo, Strains and polarization during antiferroelectric-ferroelectric phase switching in $Pb_{0.99}Nb_{0.02}[(Zr_{0.57}Sn_{0.43})_{1-y}Ti_y]_{0.98}O_3$ ceramics, J. Am. Ceram. Soc. 94 (2011) 1149–1155.
[31] C.T. Blue, J.C. Hicks, S.E. Parks, S. Yoshikawa, L.E. Cross, In situ x-ray diffraction study of the antiferroelectric-ferroelectric phase transition in PLSnZT, Appl. Phys. Lett. 68 (1996) 2942–2944.
[32] M. Ahtee, A.M. Glazer, Lattice parameters and tilted octahedral in sodium-potassium niobate solid solutions, Acta Crystallogr. 32 (1976) 434–446.
[33] A.M. Glazer, H.D. Megaw, Studies of the lattice parameters and domains in the phase transitions of $NaNbO_3$, Acta Crystallogr. 29 (1973) 489–495.